Heterogeneous Catalytic Activity of Platinum Nanoparticles Hosted in Mesoporous Silica Thin Films Modified with Polyelectrolyte Brushes

Matías Rafti,[†] Annette Brunsen,[‡,§] M. Cecilia Fuertes,[‡,⊥] Omar Azzaroni,*,[†] and Galo J. A. A. Soler-Illia*,[‡,‖]

[†]Departamento de Química, Facultad de Ciencias Exactas, Instituto de Investigaciones Fisicoquímicas Teóricas y Aplicadas (INIFTA), Universidad Nacional de La Plata, CONICET, La Plata, Buenos Aires, Argentina

[‡]Gerencia Química, Comisión Nacional de Energía Atómica, Avenida Gral Paz 1499, B1650KNA San Martín, Buenos Aires, Argentina

[§]"Soft Control", Department of Chemistry, Technische Universität Darmstadt, Petersenstrasse 22, 64287 Darmstadt, Germany

[⊥]Instituto Sabato, Universidad Nacional de San Martín, San Martín, Buenos Aires, Argentina

[‖]Departamento Química Inorgánica, Analítica y Química Física, FCEN, Universidad de Buenos Aires, Pab. II, Ciudad Universitaria, C1428EHA Buenos Aires, Argentina

Ⓢ Supporting Information

ABSTRACT: Platinum nanoparticles of 3 nm diameter were included in mesoporous silica thin films by controlling the mesopore surface charge with a short polymer brush. This metal–polymer–mesopore nanocomposite presents high catalytic activity toward ammonia oxidation at low temperatures with 4.5% weight platinum loading. An anomalous partial selectivity toward nitrous oxide is observed for the first time, which can be traced back to the synergy of the particles and modified surface. This effect opens a path toward the design of nanocomposite catalysts with highly controlled environments, in which the size- and function-controlled cavities can be tuned in order to lower the reaction barriers.

KEYWORDS: *mesoporous films, metal–polymer nanocomposites, polymer brushes, gold catalysis, ammonia oxidation, nanocatalysis*
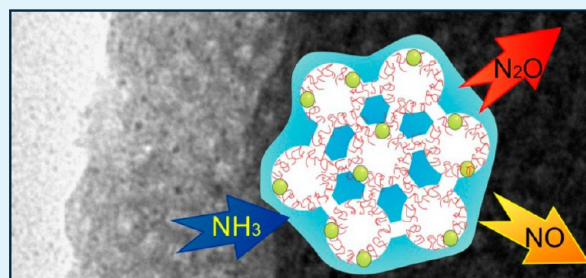
INTRODUCTION

Current research in nanocatalysis and materials science is vigorously pushing the boundaries of the systems under study into the domains of complex nanomaterials.[1−3] The core area of research in catalysis has started to shift from studies on single-crystal surfaces toward the exploration of metal nanoparticles (MNPs).[4,5] The combination of MNPs and mesoporous materials has been gaining increasing importance in heterogeneous catalysis, exploiting the exquisite control over the surface, structural and functional properties of the mesoporous supports, and high and tailorable interface area between both components.[6] Mesopores are indeed highly tuned nanoscopic environments that can influence the catalytic behavior. Beyond the expected effects of shape and size selectivity, nanoconfinement effects due to restricted volume and surface curvature result in a lowering of kinetic barriers.[7−9] Recently, a platinum−mesoporous silica catalyst prepared by impregnation allowed the attainment of fast and complete oxidation of low-pressure ethylene at ambient temperature.[10] A correlation was also recently found between the surface chemistry of the internal concave walls of mesoporous CeO₂ and the low activation energy of a water−gas shift reaction catalyzed by MNPs.[11] In addition, MNPs embedded in mesopores also exhibit excellent thermal stability under relevant turnover conditions.[12] There seems thus to be an important role of the chemical properties of the pore surface, which could be advantageously tuned in order to change the catalyst activity or selectivity.

Improving the catalytic performance through these nanocomposite systems relies on our ability to master the incorporation of MNPs into the mesoporous support. Several research efforts were recently made for devising new strategies to incorporate platinum nanoparticles (Pt NPs) into mesoporous silica for catalytic purposes. A critical aspect is the particle monodispersity and homogeneity of its incorporation.[13−17] For example, Somorjai and co-workers developed a set of protocols ranging from the hydrothermal growth of mesoporous silica in the presence of polymer-stabilized Pt NPs[18] to the sonication-aided impregnation of poly(amidoamine)-dendrimer-stabilized or poly(vinylpyrrolidone)-stabilized Pt NPs that proved very successful.[19,20] Controlled reduction methods within the mesopore system afford a
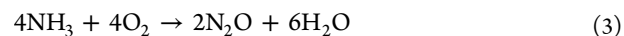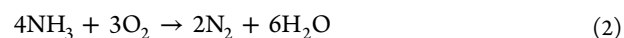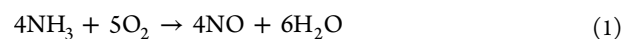
Scheme 1. Schematic Depiction of Pt NP Synthesis at the Inner Environment of a Mesoporous Silica Film[a]
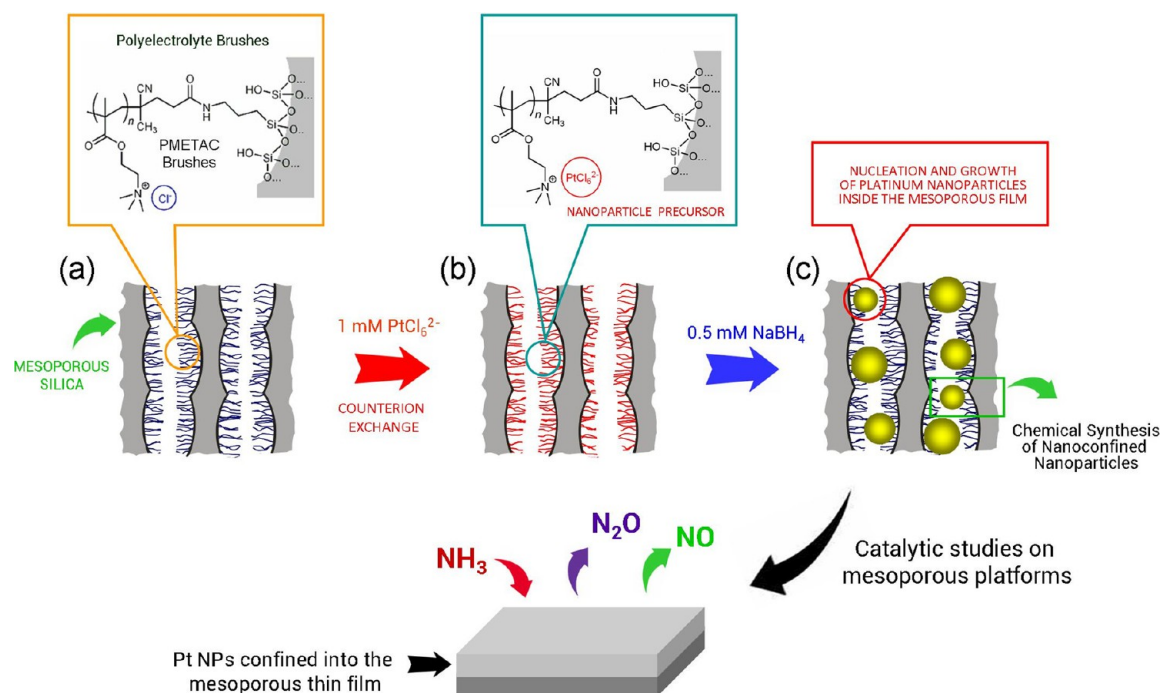
[a]The chloride counterions in the as-synthesized PMETAC-modified silica films (a) are exchanged by the corresponding anionic precursors, $PtCl_6^{2-}$ (b). Then, the platinum chloro complexes are chemically reduced to form MNPs within the nanoscale brush-coated pores (c). The scheme also describes the chemical species involved in the catalytic transformation of ammonia.

straightforward and reproducible strategy to tune the nanoparticle size and distribution by controlling the mesopore surface. The isoelectric point (IEP) of the mesoporous matrix plays a key role in the successful incorporation and dispersion of negatively charged metal precursors such as MCl_n^{z-} (M = Au, Pd, Pt, etc.) into the nanostructured support prior to reduction. Impregnation processes of $PtCl_6^{2-}$ precursors in slightly acidic conditions proceed straightforwardly in high-IEP mesoporous oxides, but the same strategy leads to very low nanoparticle loading in materials like silica (IEP ∼ 2). In order to increase the MNP loading, higher concentrations of the metal precursor or reducing agents, or harsher reduction conditions (i.e., higher temperatures, longer reaction times, etc.), are used. These conditions lead to uncontrolled growth of the metallic particles that present larger sizes and broader size dispersion, which are detrimental to the catalyst activity and selectivity. Pore modification strategies with molecular dangling amino, ammonium, or thiol groups have been applied to change the surface charge, improving impregnation of the metal precursors and thus the nanoparticle control.[21,22] In a previous work, we demonstrated that a highly controlled loading can be achieved by tethering polyelectrolyte brushes on mesoporous silica walls.[23−26] This strategy offers the possibility of supporting MNPs confined in a 3D nanometer-sized framework via simple in situ synthetic steps,[27,28] allowing the soft formation of platinum colloids locally addressed into the mesopores (Scheme 1).

In principle, confinement of Pt NPs in nanospaces can significantly change their activity and selectivity. In this work, we used the well-known heterogeneously catalyzed gas-phase oxidation of ammonia as a test of the catalytic properties of the Pt NPs hosted in the mesoporous films modified with cationic polymer brushes. Gas-phase oxidation of ammonia is an important process from both industrial and environmental viewpoints; good illustrations are nitric acid production via Ostwald process and removal of NH_3 produced in catalytic reformers of internal combustion engines.[29] Experimental and theoretical studies performed on platinum single-crystal surfaces revealed that ammonia decomposition (i.e., the initial hydrogen-atom ripping, which constitutes the highest activation energy step) is greatly accelerated by the presence of adsorbed oxygen or OH adspecies.[30−32] The same effect was also recently observed in ammonia oxidation with oxygen performed on rhodium single crystals.[33−36] Reaction products depend on several factors such as the temperature and reactant partial pressures. Over platinum catalysts, the following global reactions take place:

$$4NH_3 + 5O_2 \rightarrow 4NO + 6H_2O \tag{1}$$

$$4NH_3 + 3O_2 \rightarrow 2N_2 + 6H_2O \tag{2}$$

$$4NH_3 + 4O_2 \rightarrow 2N_2O + 6H_2O \tag{3}$$

The oxygen partial pressure was found to be the control parameter changing the preferred pathway between N_2 and nitrous oxide (NO). High temperatures and oxygen pressures favor NO formation, while the opposite results in N_2 being the preferred product. So far, ultrahigh-vacuum (UHV) single-crystal studies have shown that N_2O is produced in significant amounts only when relatively high total pressures are used (>10^{-2} mbar).[37,38]

To the best of our knowledge, this is the first study of the catalytic ammonia oxidation reaction with Pt NPs supported on mesoporous thin films near UHV regimes. NO is a greenhouse gas known to contribute to global warming approximately 300 times more than carbon dioxide (CO_2); because of these deleterious effects, further insight leading to new ways of

controlling its emissions is of great interest.[39] The approach presented here applies a well-developed toolkit, usually employed on precisely chosen monocrystalline materials to complex MNP−oxide nanocomposites. Even if the characteristics of the system explored and techniques used lead to some level of indetermination, valuable insight is gained considering that traditional methods are not suitable to precisely assess the catalytic activity and selectivity of very low quantities of nanostructured matter.

■ EXPERIMENTAL SECTION

Mesoporous nanocomposite thin film catalysts were produced in two steps. First, highly homogeneous hybrid polymeric−inorganic porous thin films (60−180 nm thickness) were produced. Subsequently, platinum salts were adsorbed within the mesopores, and Pt NPs were then obtained by mild reduction. Mesoporous aminosilica films (RNH_2:Si = 0.2:1) were deposited onto glass substrates by dip-coating, at a withdrawal speed of 2 mm/s, under 40−50% humidity. The precursor solution contains tetraethoxysilane (TEOS; Merck), (3-aminopropyl)triethoxysilane (APTES; Fluka, 98%), F127 block copolymer (Aldrich, M_r = 13600), ethanol, water, and HCl in the following molar ratio: 0.8:0.2:0.005:24:5.2:0.28 TEOS/APTES/F127/EtOH/H_2O/HCl. Pluronic F127 block copolymer was employed as the structure-directing agent. Amino-containing films were consolidated by three successive 24 h thermal treatments at 60 and 130 °C and 2 h at 200 °C (in an air atmosphere). The template was subsequently extracted by submitting to acidic ethanol (0.1 mol dm^{-3}) for 3 days, according to a previously reported protocol.[40] The surface amino functions were used as grafting sites for the surface-initiated free-radical polymerization of poly[2-(methacryloyloxy)ethyltrimethylammonium chloride] (PMETAC) brushes. In a first step, the amino groups were conjugated to 4,4′-azobis(4-cyanopentanoic acid) as a surface-confined initiator.[41] Subsequently, polymer brush polymerization was accomplished by surface-initiated free-radical polymerization of METAC monomers in a 50 wt % solution in water. Under these conditions, the aminosilica walls are negatively charged, causing a preconcentration of $METAC^+$ monomers inside the pores. The polymer content and thus the charge density can be regulated by the polymerization time. For the catalytic experiments presented below, samples submitted to 210 min of polymerization were used.

The procedure for the production of pore-embedded Pt NPs was adapted from ref 28. Briefly, in a preconcentration step, the hybrid films were immersed in an aqueous solution of 1 mM H_2PtCl_6 in H_2O (pH ∼ 2, prepared by diluting Sigma-Aldrich, 8 wt %) for 30 min. The films were then washed several times with deionized water in order to remove non-ion-paired precursors. Subsequently, in a chemical reduction step, platinum-loaded films were introduced in a 0.5 mM $NaBH_4$ solution for 30 s, rinsed with deionized water, and dried with a stream of N_2 at room temperature.

Water adsorption−desorption isotherms (at 298 K) were measured by ellipsometric porosimetry (EP; SOPRA GES5A). From the measured isotherms, pore-size distributions were obtained using models based on the Kelvin equation, considering the respective contact angles. The contact angle of water to the films was determined using a Ramé-Hart 190 CA. Field-emission scanning electron microscopy (FE-SEM) images were obtained with a ZEISS LEO 982 Gemini microscope in the secondary-electron mode; transmission electron microscopy (TEM) images were obtained with a Philips CM200 microscope with EDAX, to perform energy-dispersive spectroscopy (EDS). Grazing incidence, small-angle X-ray scattering (GI-SAXS) measurements were performed at the XRD2 beamline of Laboratório Nacional de Luz Síncrotron (LNLS), Brazil, using a six-circle Huber diffractometer and a 2D PILATUS detector (energy = 8 keV; sample-to-detector distance = 50.7 cm). The incident angle was fixed at θ = 0.2° with an integration time of 60 s. X-ray reflectometry (XRR) measurements were performed on the same LNLS beamline; in order to obtain accurate density values, measurements were performed under low-humidity conditions (under a stream of dry N_2).

Diffuse-reflectance infrared Fourier transform spectroscopy (DRIFTS) measurements were performed using a Nicolet Magna 560 instrument, equipped with a liquid-nitrogen-cooled MCT-A detector. DRIFTS measurements were performed by depositing scratched film samples on a KBr-filled DRIFTS sample holder.

The experimental setup used for monitoring the catalytic activity of Pt NPs hosted in the modified mesoporous films is similar to the one previously described for surface catalysis experiments on single-crystal surfaces.[42] The UHV chamber is pumped by a turbomolecular pump combined with an ion pump and a titanium sublimation pump. After bakeout, the system can maintain a base pressure of less than 3 × 10^{-10} mbar. A chromium−aluminum thermocouple spot-welded to the back of the sample was used for temperature measurements, and because the active material was supported on glass (which limits the maximum operating temperature to ≈350 °C), indirect heating was conducted by a tungsten filament on the back of the sample. An annealing procedure, as applied usually in UHV experiments on metallic samples, was not possible, and therefore the minimum base pressure reached was as low as 1 × 10^{-7} mbar. After several Ar^+-ion bombardments (p_{Ar} = 3 × 10^{-5} mbar) and heat (T_{max} = 300 °C) cleaning cycles were conducted, activation of the supported nanoparticle was carried out via oxidation (O_2) and reduction (H_2) cycles of approximately 40 min at 250 °C, using pressures of 1 × 10^{-5} mbar. To ensure the effectiveness of the cleaning procedure applied, reaction/cleaning cycles were repeated until subsequent measurements of the catalytic activity displayed no difference. An analogous procedure was also employed by Somorjai and co-workers to remove the polymeric capping layer.[12] The reaction rates were obtained using a differentially pumped quadrupole mass spectrometer, which was connected to a cone brought approximately 1 mm in front of the catalytically active surface, avoiding in this way any spurious signals coming from the hot filament or other parts of the experimental setup. Signals corresponding to m/e 18, 28, 30, and 44 were followed (as was usually done for experiments on the same reaction system) in order to determine the amounts of H_2O, N_2, NO, and N_2O, respectively, produced for a given reaction regime.

■ RESULTS AND DISCUSSION

Mesoporous thin films produced in the conditions reported above display highly organized pore arrays with cubic-derived mesostructure ($Im3m$) with a cubic cell parameter a of 19.6 nm, as assessed by SAXS; uniaxial contraction results in ellipsoidal-shaped pores (Figure 2). The pore size and pore volume were extracted from the water adsorption−desorption isotherms obtained from EP shown in Figure 1. EP measurements of the
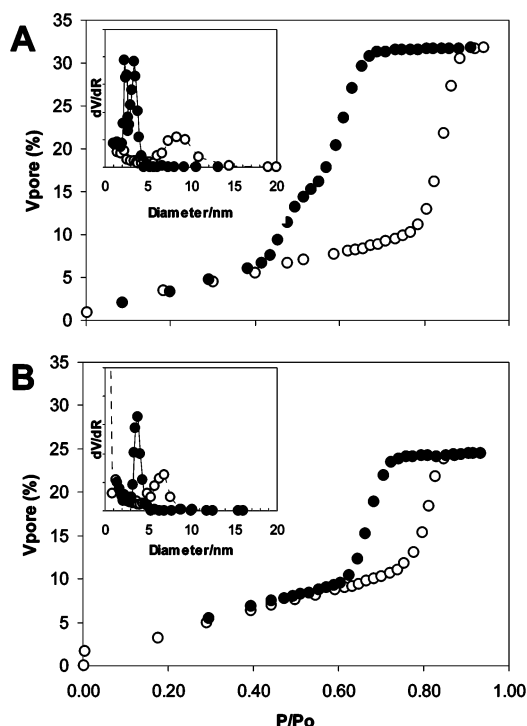
Figure 1. Water adsorption−desorption isotherms, obtained by EP, of silica thin films containing a propylamino function (A) and PMETAC brushes after 210 min of polymerization time (B). The insets in each panel correspond to the pore-size distribution of both samples. Open symbols correspond to adsorption (inset: pore size), and closed symbols correspond to desorption (inset: neck size).

amino-functionalized silica films yield 32% pore volume, and an average major pore diameter of 8.3 nm, calculated from the isotherm adsorption branch taking into account a contact angle of 30° (Figure 1A). This is in good agreement with the SEM micrographs (see the Supporting Information, SI). A two-step desorption branch is observed in the initial hybrids; this could be due, in principle, to either inhomogeneities of the mesopore structure or the existence of some pore plugging, which can lead to two different neck sizes. Structural analysis by TEM and SAXS ruled out inhomogeneities; therefore, we concluded that a fraction of the necks could correspond to pore plugging, probably by some remaining surfactant. Analysis of the isotherm desorption branch was performed according to the model proposed by Boissière et al.,[43] leading to neck sizes of 3.4 and 2.3 nm diameter.

After polymerization, the silica films presented a contact angle of 61°, corresponding to a more hydrophobic surface. EP measurements performed on PMETAC-containing samples yielded significant differences. The film pore volume decreased to 24% and the pore diameter to 6.8 nm; a unique neck size of 3.8 nm was obtained from the desorption curve (see Figure 1B). The slight neck enlargement and disappearance of the smaller neck fraction are probably a consequence of complete template extraction after the polymerization step, which is performed in a polar medium; some extra condensation leading to pore rearrangement cannot be ruled out. From these measurements, it can be concluded that a significant fraction of the mesopore volume is filled with the polymer, albeit leaving necks large enough for the swift diffusion of molecular species. The pore volume obtained by EP is in good agreement with
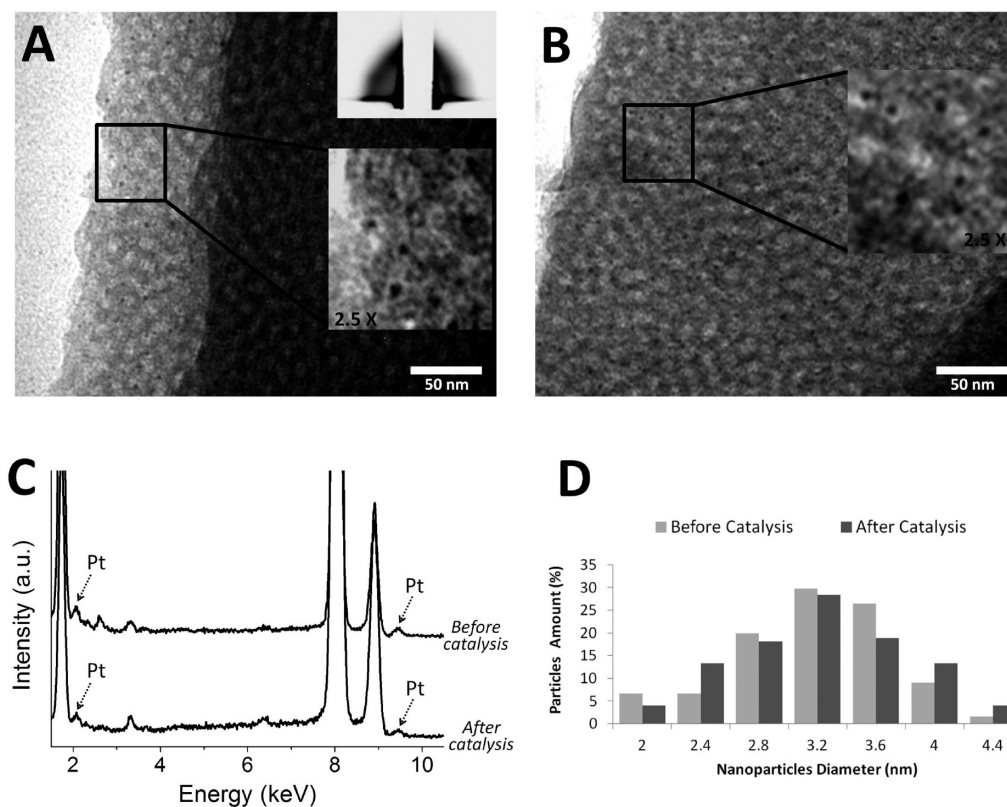

Figure 2. TEM micrographs of platinum-loaded mesoporous silica before (A) and after (B) one catalytic cycle. The inset in part A shows a GI-SAXS pattern; details (2.5×) of the nanoparticles are shown in both panels. EDS spectra of films (C) and particle-size distributions of Pt NPs (D) before and after catalysis (counting 300 nanoparticles).
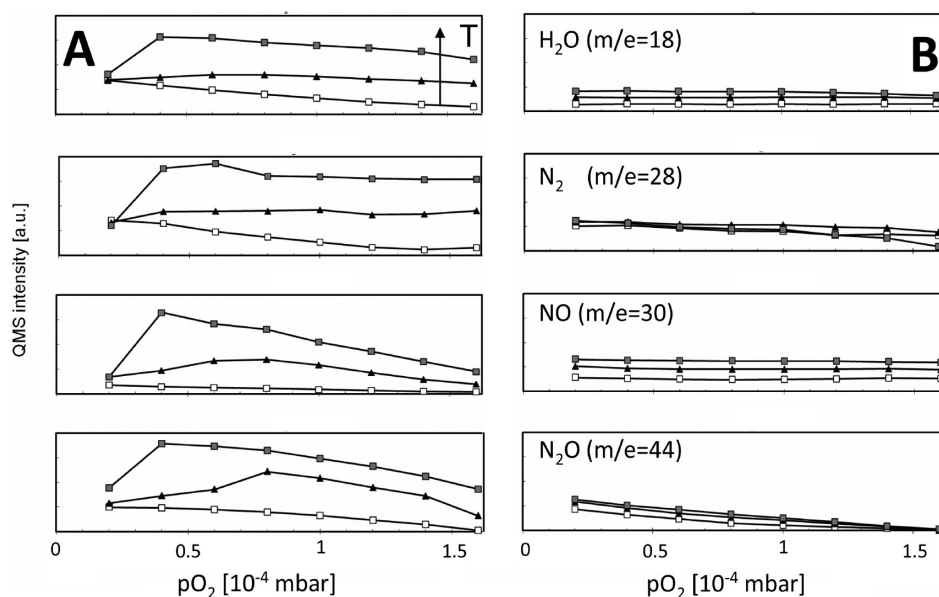
Figure 3. (A) Plot of the TOF (arbitrary units) for different reaction products versus oxygen partial pressure ($\times 10^{-4}$ mbar), for increasingly higher temperatures. All of the experiments were carried out using a fixed ammonia pressure of 4×10^{-5} mbar. Ambient temperature (30 °C) was taken as the reference for no catalytic activity and therefore is not shown. A TOF peak can be observed when the reactant ratio is approximately 1:1. (B) Same experiments as those described in part A but using a bare mesoporous support material sample. Catalytic measurements correspond to 90 (□), 140 (▲), and 220 (gray □) °C.

XRR measurements that estimate that the polymer occupies 10% of the pore volume. These results allow one to estimate an average polymerization degree of $n \approx 4.5$, according to a previous determination of the amino content in PMETAC-modified films, in which an 83% of pore filling afforded an n of ca. 30–32.[28]

The PMETAC polymer incorporated is just enough to switch the surface charge, endowing a positive charge to the pores at moderately acidic pH values. This permits the incorporation of $PtCl_6^{2-}$ and its subsequent mild reduction to Pt NPs. The presence of PMETAC was confirmed by DRIFTS (see the SI, Figure 1). A slight tint change is observed after $PtCl_6^{2-}$ reduction, suggesting that a reduction reaction takes place. TEM images of the films submitted to this reduction cycle show that MNPs with an average diameter of 3.0 ± 0.6 nm (obtained by counting 300 particles; Figure 2D) are located within the mesopores (Figure 2A).

The Pt NPs occupy less than 2% pore volume, as estimated from analysis of the XRR critical-angle shift (see the SI, Figure 2a). The metal content was determined following the procedure described in ref 44. Briefly, a change in the electronic density (ρ) of the films due to the presence of MNP implies a shift in the critical angle θ_c. From the critical-angle measurements, the electronic density of the film after and before platinum infiltration can be directly calculated using eq 1

$$\rho = \pi \theta_c^2 / \lambda^2 r_e \qquad (1)$$

where λ is the X-ray wavelength and r_e is the classical radius of the electron. Finally, we can determine the volume fraction of the Pt NPs (F_{Pt}) using eq 2:

$$F_{Pt} = (\rho_{film+Pt} - \rho_{film}) / \rho_{Pt} \qquad (2)$$

where ρ_{film} is the electronic density of the film before infiltration, $\rho_{film+Pt}$ is the electronic density of the film after platinum infiltration, and ρ_{Pt} is the platinum electronic density (4.1414×10^{24}).

The platinum loading value obtained using XRR is consistent with the 2:98 Pt/Si atomic ratio obtained by EDS (Figure 2C), which corresponds to a mass content of approximately 4.5% of platinum in the nanocomposite samples. SEM analysis of the whole sample did not detect MNP located on the outer film surface (see the SI, Figure 3). This result stresses the importance of the preconcentration of negatively charged platinum(II) precursors within the pore system, probably because of the much larger pore surface area. In a previous work, we demonstrated that pore topology and surface functionalization can indeed be used as synthetic tools to precisely locate MNPs within the mesopores rather than at the film surface.[28] In this way, robust mesopore–metal nanocomposite catalysts with accessible porosity on the order of 20% were produced in situ, as demonstrated by the water uptake observed by XRR of samples submitted to low and high relative humidity conditions (see the SI, Figure 2b). It is worth noting that the very mild conditions presented here lead to the highly localized and controlled growth of small platinum particles only in polymer-modified mesopores. Indeed, the bare silica surface and $PtCl_6^{4-}$ present negative charge for pH > 2, leading to an insignificant metal adsorption within the pores for a wide range of adsorption–reduction conditions. In order to obtain Pt NPs on pure mesoporous silica, higher concentrations of the metal salt or the reducing agent, or higher temperatures or longer reduction times, are typically used. Normally, these harsher conditions lead to uncontrolled growth of the metallic particles, and larger particle sizes with larger size distributions are obtained. This is an issue regarding the preparation of completely comparable samples containing small, controlled Pt NPs within the nonmodified silica mesopores.

Regarding measurements of the catalytic activity, it is important to stress that the active surface area of the material depends on the metal loading in the mesoporous matrix. This amount is small compared to the reactor volume (approximately 80 L). Because of this fact, high sensitivity to

contamination can be expected. This could result in a misleading interpretation of the experimental results in the sense that a good catalyst may appear to be inactive either because of contamination or because it was in an inactive state at the time of measurement. For this reason, every experiment was compared with a baseline obtained using a similar polymer-modified mesoporous silica film without Pt NPs (inactive). For the reasons discussed above, we chose ammonia oxidation as our probe reaction, and we explored different partial pressures and temperatures to assess changes in the reactivity and selectivity observed compared with the results obtained using single crystals. Given the great amount of possible regimes in terms of reactant partial pressures and temperatures, we have chosen a particular domain of these variables in which platinum is catalytically active according to previous experiments performed on platinum single-crystal surfaces. Namely, a constant ammonia partial pressure was set to 4×10^{-5} mbar, temperatures used were 90, 140, and 220 °C, and oxygen partial pressures used were in the range between 2×10^{-5} and 1.5×10^{-6} mbar.[45,46] An additional problem arises when m/e 44 is considered, which corresponds to both CO_2 and N_2O molecules. Given the polymer content of the sample, one cannot, in principle, rule out some CO_2 contribution to the m/e 44 signal, which would obscure the assessment of the catalytic activity. To avoid this uncertainty, we have performed blank experiments using the mesoporous silica film without Pt NPs in order to estimate the contribution of CO_2. In this way, we were able to obtain N_2O production for the Pt NP-containing sample by subtracting both signals. It is worth noting that the polymer integrity is maintained after catalytic measurements because FTIR signals corresponding to the polymer are observed in samples analyzed after catalysis (see the SI, Figure 1). Parts A and B of Figure 3 show the kinetic measurements performed on the mesoporous silica thin films with and without Pt NPs, respectively. The evident difference in the profiles for the m/e 44 signal between parts A and B of Figure 3 can only be due to ammonia oxidation reaction, producing N_2O.

Catalysis experiments were carried out for increasingly higher temperatures; ambient temperature (30 °C) was considered as a reference for no catalytic activity, and therefore the intensity of the quadrupole mass spectrometry (QMS) signal at any higher temperature was obtained by subtracting such a reference value. For a platinum single-crystal catalyst, a marked selectivity shift is observed depending on whether the conditions correspond to O_2 (preferred products NO and H_2O) or NH_3 (preferred products N_2 and H_2O) excess on the reactant mixture feed.[23] Differently, results obtained using Pt NPs demonstrated that, upon increasing oxygen partial pressure for any given temperature, the production rate of all of the monitored species showed a maximum value for an NH_3/O_2 ratio close to 1:1. Two striking features can be observed when parts A and B of Figure 3 are compared: first, there is evident measurable catalytic activity of the mesoporous silica film containing Pt NPs, even at relatively low temperatures; second, there is considerable production of N_2O in the same regime where the other reaction products are formed. This latter aspect is surprising provided that this catalytic behavior was not previously observed in any experiment performed on this pressure regime over platinum single-crystal surfaces.

It can be hypothesized that, aside from the reaction mechanism operating on platinum single-crystal surfaces,[47] which were analyzed elsewhere and provide a plausible explanation for selectivity toward N_2 or NO, Pt NPs confined in mesopores are able to increase the yield of N_2O through different active catalytic sites not present on single-crystal geometries. Furthermore, it is likely that the above-mentioned differences arise as a result of deviations from the simplistic Langmuir–Hinshelwood (adsorption–desorption) reaction assumed in single-crystal catalysts.

Interestingly, no change in the nanoparticle size was observed by TEM or XRR after successive catalytic cycles. A Student's t test performed over the nanoparticle size histograms before and after reaction does not show statistically significant differences, with a confidence level $p < 0.05$. This demonstrates that nanoparticles trapped inside the pore systems exhibit high stability and that the catalyst is potentially recyclable. Current efforts are directed toward testing the long-term catalytic activity of these nanocomposites.

A marked reactivity increase as the temperature increases is observed in all of the experiments. Surprisingly, a marked decrease in NO production is observed as the oxygen proportion in the reactant mixture increases, contrary to what was observed in previous experiments performed on platinum single crystals.[37]

Absolute values for the turnover frequency (TOF, expressed as product molecules formed per square centimeter per second) were estimated following the same procedure as that used for ammonia oxidation over single-crystal catalysts (see refs 37 and 38). Interestingly, these values were found to be in the 10^{14}–10^{15} s^{-1} cm^{-2} range, which is comparable to the ones found for single-crystal experiments. The applied TOF calculation procedure makes use of the collision frequency, as derived from kinetic gas theory, and assumes that the surface density of catalytically active sites is equal to the number of metallic surface atoms exposed for a certain crystallographic orientation. Despite the uncertainty of these two factors introduced because of the rugosity of the mesoporous support, the nonuniform size and spatial distribution, and the polycrystallinity of the active Pt NPs (approximately 4.5% by weight), the TOF estimations mentioned above constitute a promising result regarding the catalytic activity of this new material. Bearing in mind the limitations discussed, one can also estimate the selectivity changes when the oxygen partial pressure and temperature are increased. For the complete parameter range explored, N_2 remains the preferred product and displays an almost constant TOF value as the oxygen pressure is increased for the highest temperature tested (220 °C), as can be observed in Figure 3. Both NO and N_2O production, as measured via QMS signals, represent approximately 40–50% of the molecular nitrogen production. For the low end of the temperatures and oxygen pressures used, the ratio (NO/N_2O) remains near (1:1), and as higher temperatures and pressures are used, the selectivity shifts toward an increase in NO production up to a ≈1:0.6 ratio.

■ CONCLUSIONS

In this work, a straightforward and reproducible method to insert Pt NPs with potentially tunable catalytic activity within a controlled mesoporous environment is presented. This method is based on the tailored control of the mesopore surface. In the first step, METAC$^+$ monomers readily adsorb onto the silica surface, permitting the development of a short-chain polymer preferentially within the pore volume. In the second step, the platinum(IV) precursor anions adsorb onto the positively charged surface, and an ensuing soft reduction method grants the controlled formation of MNPs within the mesopores. The

system presents high catalytic activity even at low temperatures with low platinum loading (ca. 4.5% by mass), demonstrating the high accessibility of the heterogeneous catalyst. An anomalous partial selectivity toward NO is observed for the first time, which can be attributed to a synergetic effect between the nanoparticles and modified surface. This effect opens a path toward the nanodesign of nanocomposite catalysts with highly controlled environments, in which the synergy of thoroughly size- and function-controlled cavities can be tuned in order to lower the reaction barriers and lead to sustainable catalysts by design.

Ammonia oxidation over single-crystal and polycrystalline platinum catalysts involves the formation of NO in an intermediate step. Whether NO desorbs as a final product or participates in further reaction steps depends on a number of factors such as adsorption energies (i.e., the number and type of surface sites available in the catalyst), reactant partial pressures, and coverage of other adspecies (specifically O-ads). In this preliminary study, we have observed a considerable reduction of temperature for measurable catalytic activity, together with an increase in the N_2O proportion on the products. This illustrates that the hybrid/nanocomposite materials presented here have a great potential to tune the catalytic properties of confined Pt NPs in order to achieve different reaction products. We attribute the observed selectivity shift toward NO production to be closely related to an increment of the oxygen supply to the reaction system generated by the polymer support of Pt NPs. We anticipate that engineering different pore sizes or changing the polymer nature or amount within the mesopores will result in different particle densities and particle–matrix interactions. The systematic exploration of nanoparticle confinement and interactions with tailored hybrid mesoporous matrixes and its consequences in the catalytic activity will bring out further insight that can be used in a rational fashion for novel catalyst design.

ASSOCIATED CONTENT

Ⓢ Supporting Information
FTIR and XRR patterns of hybrid and platinum-laden mesoporous thin films and a representative FE-SEM top-view micrograph of a platinum-loaded polymer–silica film. This material is available free of charge via the Internet at http://pubs.acs.org.

AUTHOR INFORMATION

Corresponding Authors
*E-mail: azzaroni@inifta.unlp.edu.ar.
*E-mail: gsoler@cnea.gov.ar.

Notes
The authors declare no competing financial interest.

ACKNOWLEDGMENTS

REFERENCES

(1) *Surface and Nanomolecular Catalysis*; Richards, R., Ed.; CRC Press: Boca Raton, FL, 2006.
(2) *Nanocatalysis*; Heiz, U., Landman, U., Eds.; Springer-Verlag: Heidelberg, Germany, 2006.
(3) *Nanoparticles and Catalysis*; Astruc, D., Ed.; VCH-Wiley: Weinheim, Germany, 2007.
(4) *Catalysis and Electrocatalysis at Nanoparticle Surfaces*; Wieckowski, A., Savinova, E. R., Vayenas, C. G., Eds.; Marcel Dekker: New York, 2003.
(5) *Nanotechnology in Catalysis*; Zhou, B., Hermans, S., Somorjai, G. A., Eds.; Springer Science: New York, 2004; Vol. 1.
(6) For example, see the special issue Functional Porous Materials: Luque, R.; Garcia-Martinez, J. *ChemCatChem* **2013**, *5* (4), 825−1031.
(7) Centi, G.; Perathoner, S. *Coord. Chem. Rev.* **2011**, *255*, 1480−1498.
(8) Díaz, U.; Brunel, D.; Corma, A. *Chem. Soc. Rev.* **2013**, *42*, 4083−4097.
(9) Huang, S.; Hara, K.; Fukuoka, A. *Energy Environ. Sci.* **2009**, *2*, 1060−1068.
(10) Jiang, C.; Hara, K.; Fukuoka, A. *Angew. Chem., Int. Ed.* **2013**, *52*, 6265−6268.
(11) Wen, C.; Zhu, Y.; Ye, Y.; Zhang, S.; Cheng, F.; Liu, Y.; Wang, P.; Tao, F. *ACS Nano* **2012**, *6*, 9305−9313.
(12) Rioux, R. M.; Song, H.; Hoefelmeyer, J. D.; Yang, P.; Somorjai, G. A. *J. Phys. Chem. B* **2005**, *109*, 2192−2202.
(13) Datta, K. K. R.; Reddy, B. V. S.; Ariga, K.; Vinu, A. *Angew. Chem., Int. Ed.* **2010**, *49*, 5961−5965.
(14) Fukuoka, A.; Kimura, J.-I.; Oshio, T.; Sakamoto, Y.; Ichikawa, M. *J. Am. Chem. Soc.* **2007**, *129*, 10120−10125.
(15) Huang, T.; Tu, W. *Appl. Surf. Sci.* **2009**, *255*, 7672−7678.
(16) Prashar, A. K.; Mayadevi, S.; Rajamohanan, P. R.; Nandini Devi, R. *Appl. Catal., A* **2011**, *403*, 91−97.
(17) Zhu, J.; Xie, X.; Carabineiro, S. A. C.; Tavares, P. B.; Figueiredo, J. L.; Schömäcker, R.; Thomas, A. *Energy Environ. Sci.* **2011**, *4*, 2020−2024.
(18) Song, H.; Rioux, R. M.; Hoefelmeyer, J. D.; Komor, R.; Niesz, K.; Grass, M.; Yang, P.; Somorjai, G. A. *J. Am. Chem. Soc.* **2006**, *128*, 3027−3037.
(19) Witham, C. A.; Huang, W.; Tsung, C.-K.; Kuhn, J. N.; Somorjai, G. A.; Toste, F. D. *Nat. Chem.* **2010**, *2*, 26−41.
(20) Kuhn, J. N.; Huang, W.; Tsung, C.-K.; Zhang, Y.; Somorjai, G. A. *J. Am. Chem. Soc.* **2008**, *130*, 14026−14027.
(21) Gutiérrez, L.-F.; Hamoudi, S.; Belkacemi, K. *Catalysts* **2011**, *1*, 97−154.
(22) Yang, C.-M.; Liu, P.-H.; Ho, Y.-F.; Chiu, C.-Y.; Chao, K.-J. *Chem. Mater.* **2003**, *15*, 275−280.
(23) Brunsen, A.; Díaz, C.; Pietrasanta, L. I.; Yameen, B.; Ceolín, M.; Soler-Illia, G. J. A. A.; Azzaroni, O. *Langmuir* **2012**, *38*, 3583−3592.
(24) Brunsen, A.; Cui, J.; Ceolín, M.; del Campo, A.; Soler-Illia, G. J. A. A.; Azzaroni, O. *Chem. Commun.* **2012**, *48*, 1422−1424.
(25) Calvo, A.; Yameen, B.; Williams, F. J.; Soler-Illia, G. J. A. A.; Azzaroni, O. *J. Am. Chem. Soc.* **2009**, *131*, 10866−10868.
(26) Calvo, A.; Yameen, B.; Williams, F. J.; Azzaroni, O.; Soler-Illia, G. J. A. A. *Chem. Commun.* **2009**, 2553−2555.
(27) Azzaroni, O.; Soler-Illia, G. J. A. A. *Chem. Soc. Rev.* **2011**, *40*, 1107−1150.
(28) Calvo, A.; Fuertes, M. C.; Yameen, B.; Williams, F. J.; Azzaroni, O.; Soler-Illia, G. J. A. A. *Langmuir* **2010**, *26*, 5559−5567.
(29) Chilton, T. H. In *The manufacture of nitric acid by the oxidation of ammonia*; Chemical Engineering Progress Monograph Series; American Institute of Chemical Engineers: New York, 1960; Vol. 56, Issue 3.
(30) Novell-Leruth, G.; Ricart, J. M.; Pérez-Ramírez, J. *J. Phys. Chem. C* **2008**, *112*, 13554−13562.

8839

dx.doi.org/10.1021/am403836f | *ACS Appl. Mater. Interfaces* 2013, 5, 8833−8840

(31) Offermans, W. K.; Jansen, A. P. J.; van Santen, R. A.; Novell-Leruth, G.; Ricart, J. M.; Pérez-Ramírez, J. *J. Phys. Chem. C* **2007**, *111*, 17551−17557.

(32) Offermans, W. K.; Jansen, A. P. J.; van Santen, R. A. *Surf. Sci.* **2006**, *600*, 1714−1734.

(33) Rafti, M.; Lovis, F.; Imbihl, R. *Catal. Lett.* **2012**, *142*, 16−21.

(34) Rafti, M.; Uecker, H.; Lovis, F.; Krupennikova, V.; Imbihl, R. *Phys. Chem. Chem. Phys.* **2012**, *14*, 5260−5264.

(35) Imbihl, R.; Scheibe, A.; Zeng, Y. F.; Günther, S.; Kraehnert, R.; Kondratenko, V. A.; Baerns, M.; Offermans, W. K.; Jansen, A. P. J.; van Santen, R. A. *Phys. Chem. Chem. Phys.* **2007**, *9*, 3522−3540.

(36) Imbihl, R.; Scheibe, A.; Lins, U. *Surf. Sci.* **2005**, *577*, 1−14.

(37) Bogicevic, A.; Hass, K. C. *Surf. Sci. Lett.* **2002**, *506*, L237−L242.

(38) Kraehnert, R.; Baerns, M. *Chem. Eng. J.* **2008**, *137*, 361−375.

(39) Ravishankara, A. R.; Daniel, J. S.; Portmann, R. W. *Science* **2009**, *326*, 123−125.

(40) Calvo, A.; Angelome, P. C.; Sanchez, V. M.; Scherlis, D. A.; Williams, F. J.; Soler-Illia, G. J. A. A. *Chem. Mater.* **2008**, *20*, 4661.

(41) Huang, W.; Skanth, G.; Baker, G. L.; Bruening, M. L. *Langmuir* **2001**, *17*, 1731.

(42) Rafti, M.; Lovis, F.; Zeng, Y. F.; Imbihl, R. *Chem. Phys. Lett.* **2007**, *446*, 323−328.

(43) Boissière, C.; Grosso, D.; Lepoutre, S.; Nicole, L.; Brunet-Bruneau, A.; Sanchez, C. *Langmuir* **2005**, *21*, 12362.

(44) Fuertes, M. C.; Marchena, M.; Marchi, M. C.; Wolosiuk, A.; Soler-Illia, G. J. A. A. *Small* **2009**, *5*, 272−280.

(45) Kim, M.; Pratt, S. J.; King, D. A. *J. Am. Chem. Soc.* **2000**, *122*, 2409−2410.

(46) Bradley, J. M.; Hopkinson, A.; King, D. A. *J. Phys. Chem.* **1995**, *99*, 17032−17042.

(47) Guthrie, W. L.; Sokol, J. D.; Somorjai, G. A. *Surf. Sci.* **1982**, *109*, 390−418.